AIAA JOURNAL
Vol. 43, No. 4, April 2005

Probabilistic Structural Optimization Under Reliability, Manufacturability, and Cost Constraints

Masoud Rais-Rohani* and Qiulin Xie†
Mississippi State University, Mississippi State, Mississippi 39762

A methodology is presented for probabilistic design optimization of aircraft structures subject to a set of multidisciplinary constraints including reliability, manufacturability, and manufacturing cost. Using the advanced first-order second-moment method, reliability of each structural component is evaluated by considering its primary static failure mode. Metrics-based analytical models are used in manufacturability analysis, and semi-empirical models are used for manufacturing cost estimation. The described design methodology is developed into a software tool and applied to probabilistic sizing optimization of a moderately loaded built-up wing spar. Using two alternative web design concepts, one limited by buckling and the other by diagonal semitension field action, the spar model is optimized for weight considering uncertainties in the material properties, structural sizing, and loading parameters. The optimization problem is solved using the method of sequential quadratic programming for different values of target reliability, with or without any limit on manufacturing cost. The optimization results are used to highlight the interactions between reliability, weight, and cost, whereas the probabilistic sensitivities are used to examine the influence of each random variable on structural reliability.

Introduction

THE successful design and development of any aircraft depends, in large extent, to the quality and efficiency of its structural system. In an effort to optimize the structure for weight, it is possible to reach a design that has an unacceptable level of reliability or is too expensive to manufacture. Therefore, in preliminary design of aircraft structures, it is necessary to account not only for strength and weight, but also a host of other attributes, including reliability, producibility, and affordability, which can have a significant influence on the overall quality of the aircraft.

A formidable challenge in addressing such design requirements as producibility and affordability is the development of mathematical models that can quantitatively and accurately describe the relationships between variables controlled by the designer and parameters defining the capabilities of the manufacturing process and the production costs. Traditionally, design rules based on qualitative measures of manufacturability and production cost are used to help the designer identify and eliminate design features that can adversely impact the product manufacture. Although these qualitative measures are helpful in promoting design-for-manufacturing standards, they cannot be easily translated into constraint functions that can be used in mathematical formulation and solution of the ensuing design optimization problem. In contrast, many researchers have developed what could be characterized as high-fidelity physics-based computational models, each applicable to a specific manufacturing process. Gupta et al.[1] describe some of these manufacturability analysis techniques and the efforts that are underway to automate and integrate them into computational design tools. Although very sophisticated and accurate, these high-fidelity analysis procedures are rather computationally intensive and require detailed geometric information, which is ordinarily not available at the preliminary design phase. Other researchers, such as Kessler et al.,[2] describe producibility methodology and virtual manufacturing as effective means of addressing manufacturing requirements in product design. Their strategy is based on a hierarchical producibility framework focusing on critical components and manufacturing processes. Virtual manufacturing is used for computer modeling of key manufacturing processes and functions that are defined as constraints from the standpoint of capacity or capability.

Considering the myriad of manufacturability analysis techniques, a more pragmatic approach, from the design optimization standpoint, is one that describes the manufacturability requirements in terms of metrics that relate process physics to geometric (shape and sizing) attributes of a structural part which can be adjusted during the optimization process. Although lacking the fidelity and sophistication of more advanced manufacturability analysis schemes, the metric-based techniques use analytical functions with sufficient degree of accuracy for many preliminary design applications.

Shankar and Jansson[3] developed a metrics-based methodology that can be used for producibility analysis of any manufactured product based on what they describe as five core manufacturability concepts and the hierarchy of factors on which each concept depends. In promoting the use of metrics for process-physics-dominated processes, Subramaniam and Ulrich[4] presented a technique for quantitative producibility analysis of extruded parts. They identified seven metrics relating several different failure modes or producibility problems that can be encountered during the extrusion process to various geometric properties of the extruded part. Some of the metrics they describe are used in this research for the formulation of manufacturability constraints with details to appear later in the paper. Other efforts in this area include the work by Fenyes[5] who used forming strain and elastic recovery (i.e., springback) to introduce formability constraints in design optimization of structural parts manufactured using the stamping process.

Production cost is used here as a measure of design affordability and, as in the case of manufacturability, it is a difficult response to model. A review of literature indicates that most manufacturing cost models can be classified under two categories: parametric-cost (PC) and manufacturing-process-cost (MPC) estimating models. Among the proposed PC models, a good example is that developed by Dean[6] in which the normalized manufacturing cost is expressed, in the form of power law, as a function of the number and values of product/process parameters that contribute to cost. Unlike the PC, the

Presented as Paper 2003-1631 at the AIAA/ASME/ASCE/AHS 44th Structures, Structural Dynamics, and Materials Conference, Norfolk, VA, 7–10 April 2003; received 26 December 2003; revision received 3 November 2004; accepted for publication 9 November 2004.

*Professor, Department of Aerospace Engineering. Associate Fellow AIAA.

†Graduate Research Assistant; currently Graduate Student, George W. Woodruff School of Mechanical Engineering, Georgia Institute of Technology, Atlanta, GA 30332-0405.

MPC models are not suitable for most preliminary design applications as they require in-depth specification of part geometry (shape and size) and the manufacturing process.

To facilitate the inclusion of manufacturing cost in early stages of aircraft structural design, the Air Force Wright Aeronautical Laboratories initiated a program in the late 1970s to develop what became known as the Manufacturing Cost/Design Guide (MC/DG). That program involved the participation of several aerospace companies and resulted in the publication of a series of reports by its principal contractor, Battelle Columbus Laboratories. Those reports contain information on cost-driver elements, cost-estimating data, and relative recurring and nonrecurring tooling cost estimates for the manufacture of certain discrete aerospace parts as well as for mechanically fastened structural assemblies. The cost-estimation models used in the present study are mostly based on the general information and empirical relationships contained in a subset of published MC/DG reports.[7–10]

Unlike manufacturability analysis and manufacturing cost estimation, structural reliability is a fairly mature field. There are many random sampling, analytical, and hybrid techniques with varying degrees of complexity, sophistication, and accuracy that can be used to estimate the probability of failure of a structural system as well as its individual components. In this research, the focus is on component reliability based on an advanced first-order reliability analysis technique, with details described later in the paper.

Inherent variations in the applied loads and material properties coupled with deviations in geometric dimensions introduced during the manufacturing process lead to structural design uncertainties. The traditional deterministic design optimization methods do not account for such uncertainties and can result in designs that have higher failure probabilities than expected. The desire to manage design uncertainties and to reduce their impact on structural safety has led to the development of nondeterministic (e.g., probabilistic) design methods and the emergence of reliability-based structural optimization (RBSO). Besides providing a brief history of RBSO, Frangopol[11] describes various ways of formulating and solving an RBSO problem with the help of multiple examples.

The work presented in this paper is an extension of previous efforts[12,13] that focused on the mathematical modeling of manufacturability and cost constraints and their inclusion in deterministic optimization of aircraft structures with a single- or multi-objective function formulation. The principal research thrust here is the development of a probabilistic optimization approach to account for design uncertainties and their influence on structural reliability. Besides reliability against failure in individual structural components, design manufacturability and manufacturing cost form the primary constraints.

The described approach is demonstrated through the formulation and solution of a built-up wing spar design optimization problem where the structural sizing and applied load parameters along with the material properties are treated as random variables. The resulting single-objective, multiconstrained optimization problem is solved for minimum weight based on two alternate (i.e., buckling and nonbuckling) web design concepts with the mean values of sizing random variables selected as design variables. Whereas the methodology enables the formulation and solution of a more general probabilistic optimization problem, the wing spar example is set up and solved such that the influence of design uncertainties is captured only through the reliability constraints imposed on individual structural members. However, because the natural (i.e., achievable) tolerances, governed by the precision of the manufacturing process, determine the expected variance in sizing random variables, then the choice of manufacturing process also has an impact on component reliability. This correlation is demonstrated in the wing spar example.

In the remaining portion of the paper, we present the method of analysis for the primary design constraints followed by the description of the probabilistic optimization problem, discussion of results, and the role of cost and reliability constraints, examination of probabilistic sensitivities of reliability constraints, and conclusions.

Reliability Analysis

In its fundamental form, the probability of failure of a structural component can be expressed as

$$P_f = P[g(\boldsymbol{X}) \leq 0] \tag{1}$$

where $\boldsymbol{X} = \{X_1, X_2, \ldots, X_n\}^T$ is an n-dimensional vector of random variables and $g(\boldsymbol{X})$ is the limit state function describing the failure criterion, such that $g < 0$ represents failure, $g > 0$ represents safety, and $g = 0$ represents the limit state boundary separating the safe and failed regions. When random variables are continuous, the failure probability is found by evaluating the multiple integral of the joint probability density function $f_X(\boldsymbol{x})$ over the failure region Ω expressed as

$$P_f = \iint \ldots \int_{\Omega} f_X(x_1, x_2, \ldots, x_n)\, \mathrm{d}x_1\, \mathrm{d}x_2 \ldots \mathrm{d}x_n \tag{2}$$

For most engineering problems involving multiple continuous random variables, the exact formulation of $f_X(\boldsymbol{x})$ and the solution of the multiple integral in Eq. (2) might not be possible. Hence, the probability of failure is usually estimated using a variety of techniques including those commonly known as the random sampling methods (e.g., Monte Carlo simulation), analytical methods (e.g., first-order reliability method), or hybrid methods (e.g., advanced mean value method combined with adaptive importance sampling[14]).

In analytical methods, the reliability index β is often taken as a surrogate for failure probability. To calculate β, in standard time-invariant structural reliability, the limit state function is transformed from its original random-variable space $g(\boldsymbol{X})$ to standard normal space $g(\boldsymbol{u})$, where $\boldsymbol{u}$ is the vector of standardized, independent normal variables. Then the most probable point (MPP) of failure, the point on $g(\boldsymbol{u}) = 0$ surface where the joint probability density function is maximum, is found by solving the following optimization problem:

$$\min \qquad |\boldsymbol{u}^*| = \sqrt{\boldsymbol{u}^T \boldsymbol{u}}, \qquad \text{s. t.} \qquad g(\boldsymbol{u}) = 0 \tag{3}$$

where $|\boldsymbol{u}^*|$ is the distance from the origin of coordinate system to MPP in u space and is commonly referred to as the reliability or safety index β.

The optimization problem in Eq. (3) can be solved using a variety of mathematical programming techniques[15] or tailored methods including those developed by Hasofer and Lind[16] and extended by Rackwitz and Fiessler[17] to problems involving nonnormal random variables.

In this research, we used the Rackwitz–Fiessler implementation of the advanced first-order second-moment (AFOSM) method for the calculation of β. This technique is deemed more accurate than the Hasofer–Lind approach, as in addition to the mean and standard deviation, it also includes the effect of probability distribution of random variables that are nonnormal. Once β is found, the probability of failure for the case $\beta > 0$ is estimated using the relationship $P_f \approx \Phi(-\beta)$, where Φ is the cumulative distribution function of the standard normal variate.

One advantage of analytical over sampling techniques is that they facilitate the calculation of probabilistic sensitivities of β with respect to the mean and standard deviation of random variable X_i represented as[18]

$$\frac{\partial \beta}{\partial \mu_{X_i}} = \left(\frac{\partial \beta}{\partial u_i}\right)\left(\frac{\partial u_i}{\partial \mu_{X_i}}\right) \tag{4a}$$

$$\frac{\partial \beta}{\partial \tilde{\sigma}_{X_i}} = \left(\frac{\partial \beta}{\partial u_i}\right)\left(\frac{\partial u_i}{\partial \tilde{\sigma}_{X_i}}\right) \tag{4b}$$

whereas the sensitivity derivatives in Eq. (4a) can help measure the influence of each random variable on β, those in Eq. (4b) quantify the effect of parametric uncertainty on component reliability.

Manufacturability Analysis

A key element in successful inclusion of manufacturability constraints in design optimization of aircraft structures is the ability to relate the failure mode or problems that can occur in the manufacturing process to the design variables. The metrics-based method facilitates the establishment of such relationships.

In this paper, we are limiting our discussion of manufacturability analysis by considering only the configuration-process compatibility[3] of extruded parts and the mechanical assembly of the structure. Configuration-process compatibility examines the relationship between cross-sectional geometry (shape and size) of an extruded part and the failure conditions in the extrusion process.

For producibility analysis of process-physics-dominated processes such as extrusion, Subramaniam and Ulrich[4] contend that feature-based methods are not adequate as individual geometric features cannot be effectively analyzed independently of each other, and it is necessary to consider the interaction of such features in determining the severity of each failure mode. They propose a metrics-based method for manufacturability analysis based on approximations of the underlying process physics.

All eight possible failure modes in the extrusion process (i.e., bending of extrusion, waviness, hot shortness, floppy shapes, die tongue breakage, distortion following heat treatment, die wear, and extrusion press limitations) depend, in part, on the cross-sectional shape and dimensions of the extruded part. Among the seven producibility metrics noted or derived by Subramaniam and Ulrich,[4] section balance, shape factor, and form factor are found to be most relevant to the present research and are included in this paper. A brief definition of each metric follows next.

As the billet material is pushed through the die at constant speed to produce the extruded part, it is subjected to the ram force with resultant acting at the centroid of the cross-sectional area (CA) as well as the equal and opposite drag force with resultant acting at the center of perimeter (CP). Because of possible eccentricity of drag and ram force resultants, it is possible for the extrusion to bend as it exits the die. The section balance (SB) is a metric that can be used to measure the bending tendency, and it is defined as the ratio of the offset between the points CA and CP to the radius of a minimum circumscribing circle. For simplicity, the distance measured from CA to the farthest point on the cross section is used as the minimum radius. As SB becomes larger, there is a greater tendency for the extrusion to bend.

Hot shortness refers to the surface tear and roughness of the extruded part as it exits the die. It occurs when the exit temperature is too close to the solidifying temperature of the alloy. The shape factor (SF) is a metric that can be used to predict the possibility of hot shortness, and it is defined as the ratio of the cross-sectional perimeter to the cross-sectional area. As SF grows, the chance for hot shortness increases.

The circumscribing circle determines the size of press required for producing the extrusion with the extrusion pressure increasing as the wall thickness is reduced. The ratio of the diameter of the minimum circumscribing circle to the minimum wall thickness is referred to as the form factor (FF), and it can be used as a predictor for required extrusion press size and pressure. The growth in FF indicates greater difficulty with the extrusion process.

Besides the preceding metrics, manufacturability requirements related to the assembly of the structure are also considered with details provided in the example problem.

Cost Estimation

As in the case of MC/DG, we define the total manufacturing cost of a discrete part as the sum of recurring and nonrecurring costs measured in units of labor hours (l-hr). The recurring labor costs include those associated with the manufacture of the part as well as its testing, inspection, and evaluation (TI&E). Furthermore, the additional cost penalty as a result of designer-influenced cost elements (DICE) is also included in estimation of the recurring cost. According to MC/DG, the manufacturing complexities that require either additional standard manufacturing operations (e.g., joggles, flanged holes, and beads) or special shop operations (e.g., heat treatment, special tolerances, and special finish) are considered as DICE. The nonrecurring cost is mainly a result of the tooling cost with some contribution from TI&E. When structural design includes the consideration of alternative material systems, the recurring cost must also include the cost of raw materials. Otherwise, it is permissible to disregard material contribution in order to focus mainly on the manufacturing labor cost.

Therefore, the manufacturing cost of a discrete part (DPC) is the sum of direct recurring (PRC) and nonrecurring (PNRC) costs of part manufacturing, with each component determined as

$$\mathrm{PRC} = (\mathrm{RC}_p + \mathrm{DICE}_p + \mathrm{RC}_{\mathrm{TI\&E}} + \mathrm{DICE}_{\mathrm{TI\&E}})\mathrm{LCF}_P \tag{5}$$

$$\mathrm{PNRC} = \mathrm{NRC}_T + \mathrm{NRC}_{\mathrm{TI\&E}} \tag{6}$$

which include the recurring labor cost (RC) of manufacturing the base part (RC_p); the additional manufacturing labor cost due to DICE (DICE_p); the RC for TI&E of the base part ($\mathrm{RC}_{\mathrm{TI\&E}}$); the additional labor cost of TI&E as a result of DICE ($\mathrm{DICE}_{\mathrm{TI\&E}}$); the learning curve factor for part manufacture (LCF_P); the nonrecurring tooling cost (NRC_T); and the nonrecurring TI&E cost ($\mathrm{NRC}_{\mathrm{TI\&E}}$).

Similar to DPC, the total assembly cost (TAC) is found as the sum of direct recurring cost (ARC) and nonrecurring cost (ANRC) of assembly, where ARC is found using an equation similar to Eq. (5), and is affected by the total number of fasteners in the assembly, method of fastener installation (e.g., manual, automatic, or combination), and whether the installation is dry or requires sealant.[10] In this case, the assembly learning curve factor (LCF_A) depends on the design quantity, and the learning curve rate associated with a particular method of assembly. The nonrecurring assembly cost (ANRC) is found using an equation similar to Eq. (6) by replacing the part-cost data with that of the assembly.[8]

Thus, the total manufacturing cost for a built-up structure is obtained as

$$\mathrm{TMC} = \sum_{i=1}^{\mathrm{NDP}} \mathrm{DPC}_i(\mathrm{DPQ}_i) + \mathrm{TAC} \tag{7}$$

where DPC_i is the manufacturing cost of the ith discrete part, DPQ_i is the quantity of ith discrete parts used in the assembly, and NDP is the number of discrete parts.

In MC/DG, the individual cost elements in Eqs. (5) and (6) are represented by separate graphs based on material type, material form, part geometry, principal manufacturing process, and the method of assembly. Hence, it is possible to develop analytical models for approximating the manufacturing cost as a function of structural design parameters. For example, in the case of end milling of aluminum parts, MC/DG provides multiple curves (designated as CED-M/C-25)[9] to estimate the recurring cost at unit 200 based on 80% rough and 20% finish machining operation. Each curve is designated by the initial material weight W_I, and it relates the recurring milling cost to the weight of material removed W_R, with both W_I and W_R measured in units of pounds. We have used these curves to generate several analytical equations for estimating the machining cost of a straight lineal structural member such as a spar cap. For instance, if $W_I < 45.4$ kg (100 lb), the RC for milling is estimated as

$$\mathrm{RC} = 38(W_R/100) \tag{8}$$

and if 45.4 kg (100 lb) $< W_I <$ 90.8 kg (200 lb), the RC equation changes to

$$\mathrm{RC} = [0.245(W_I - 100) + 38](W_R/W_I) \tag{9}$$

In MC/DG, the recurring cost estimates are based on the cost at unit 200. Therefore, to obtain the cumulative average cost for the design quantity and learning curve rate considered in each case, the 200th-unit cost is multiplied by the learning curve factor found as

$$\mathrm{LCF} = \frac{[1/Q(m+1)][(Q+0.5)^{m+1} - 0.5^{m+1}]}{200^m} \tag{10}$$

where Q is the design quantity produced and $m = \ell n(lc)/\ell n(2)$ with lc being the learning curve rate.[9]

Equations (8) and (9) do not include costs associated with setup, fixture, tooling, nonoperating time, etc. Therefore, they represent only a fraction of the true manufacturing cost. Nonetheless, these analytical models focus on the portion of manufacturing cost that is most influenced by product design. Although not exact, these cost estimates render a meaningful economic scale for comparing different design concepts in terms of relative manufacturing cost.

Probabilistic Design Optimization

In probabilistic design optimization, inherent uncertainties associated with material properties, loading condition, sizing, and strength are captured in the mathematical formulation and solution of the design problem. In its general formulation, the probabilistic optimization problem is to find the optimal values of design variables $\boldsymbol{Y} = \{Y_1, Y_2, \ldots, Y_{\text{NDV}}\}^T$ that would

$$\begin{aligned} &\min && f(\boldsymbol{Y}) = a_1\mu_f(\boldsymbol{Y}) + a_2\tilde{\sigma}_f(\boldsymbol{Y}) \\ &\text{s. t.} && P[E_i(\boldsymbol{Y})] \le P_i^0, && i = 1, 2, \ldots, N_E \\ & && Y_k^l \le Y_k \le Y_k^u, && k = 1, 2, \ldots, \text{NDV} \end{aligned} \tag{11}$$

where μ_f and $\tilde{\sigma}_f$ represent the mean and standard deviation values, respectively, of the objective function being optimized with coefficients a_1 and a_2 denoting the relative importance of corresponding terms in the optimization problem. Each of the N_E design constraints is expressed in terms of the probability of an event occurrence denoted by $P[E(\boldsymbol{Y})]$ being no greater than the specified limit P^0. For instance, an event can be defined as failure condition of a structural member, or it can represent deflection or manufacturing cost being greater than its allowable upper bound. In Eq. (11) the design variables could represent the mean and/or standard deviation values of a subset of random variables.

Using the relationship between failure probability and reliability index described earlier, it is possible to rewrite the design constraints in Eq. (11) as $\beta_i \ge \beta_i^0$, where $\beta_i = \Phi^{-1}[1 - P(E_i)]$ and $\beta_i^0 = \Phi^{-1}(1 - P_i^0)$. An example demonstrating the solution of a multiconstrained probabilistic optimization problem is presented next.

Wing-Spar Optimization Problem

The built-up wing spar in this example problem is modeled as a tapered ($H_2 = 0.5H_1$) cantilever beam under a distributed transverse load as shown in Fig. 1a. The spar consists of upper and lower caps of equal size as well as three flat web segments of equal length but different thickness that are spliced together and supported vertically by a number of web stiffeners.

The identical upper and lower spar caps start as 2024-T3 extruded Tee sections as shown in Fig. 1b. While preserving the cross-sectional symmetry, all surfaces are end milled (i.e., 80% rough and 20% finish machining) with thickness and width of the horizontal flanges allowed to decrease linearly from the root section such that $(t_{1\text{tip}}, w_{1\text{tip}}) = \text{TR}(t_1, w_1)$, where TR is the cap taper ratio. By contrast, the thickness and width of the vertical flange (t_2, w_2) are kept constant along the length. The learning curve rate for machining is taken to be 90%.

Each spar web segment is made of flat 2024-T3 aluminum sheet that is only cut to size, with the cutting process assumed to have a learning curve rate of 90%. A minimum of four vertical stiffeners is used to support the spar web, with one placed at each spar end and one at every web-splice location as shown in Fig. 1a. The angle-shaped 2024-T3 extruded web stiffeners are of equal cross-sectional dimensions and vary only in length. Based on the structural requirement of the critical panel in each web segment, one or more intermediate stiffeners are added to each segment, with placement details appearing later in the paper. Unlike the caps, the extruded web stiffeners do not require any machining and are only cut to length at a learning curve rate of 90%. Furthermore, because the

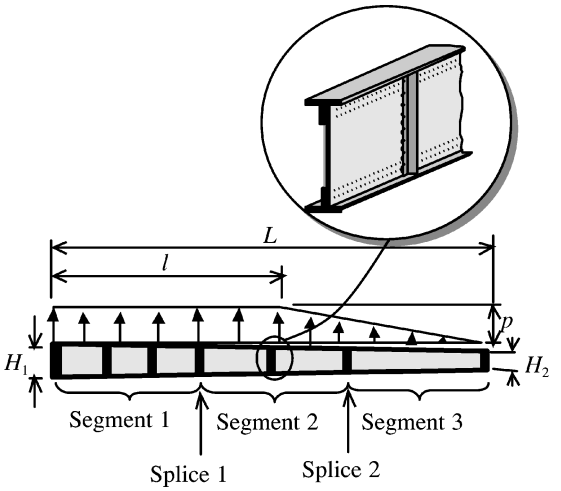

Fig. 1a Spar geometry and loading condition.

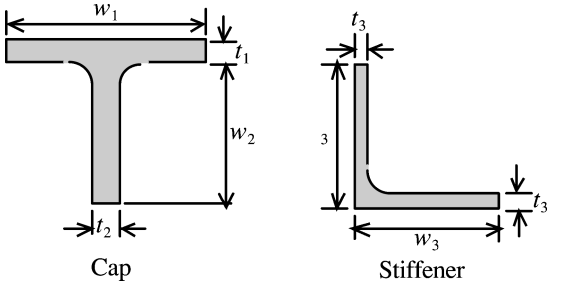

Fig. 1b Cross-sectional detail of caps and stiffeners.

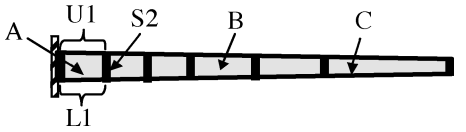

Fig. 1c Critical structural elements.

stiffeners are attached to the backside of the web (Fig. 1a), they do not require end joggles for proper attachment to the vertical flanges of the upper and lower caps. Because web thickness can vary from one segment to the next, each splice joint would require shimming as well as a doubler plate.

All parts are mechanically fastened together using 2017-T3 flathead fasteners. Although the caps are attached to the spar web and web stiffeners using two rows of fasteners with a diameter of 6.35 mm, the web stiffeners are attached to the spar web using only a single row of 4.76-mm fasteners. In both cases, the installation is assumed to be dry (i.e., without sealant). For manufacturing cost calculations, the total number of spars (i.e., design quantity) to be produced is assumed to be 50. Each spar is assembled manually with a learning curve rate of 85%.

Description of Random Variables

To account for uncertainties in structural sizing, loading condition, and material properties, the 18 parameters identified in Table 1 are treated as random variables (RVs). All RVs are assumed to be statistically independent and normally distributed with the mean values of the first eight representing the cross-sectional dimensions of the spar caps at the root (after end milling), stiffener flange dimensions, web thickness in segment 1, as well as the cap taper ratio, treated as independent design variables. As will be explained later, the mean thicknesses in web segments 2 and 3 are allowed to change in the optimization process, but they are not treated as independent design variables. The spar length and height dimensions, which are ordinarily defined by the wing span and aerodynamic shape, are also treated as random variables but are excluded from the vector of independent design variables.

Table 1 Description of independent random variables

RV no.	Definition, unit	Mean value	Standard deviation
1[a]	w_1, mm	Y_1	0.0254
2[a]	t_1, mm	Y_2	0.0254
3[a]	w_2, mm	Y_3	0.0254
4[a]	t_2, mm	Y_4	0.0254
5[a]	w_3, mm	Y_5	$0.01Y_5$
6[a]	t_3, mm	Y_6	$0.01Y_6$
7[a]	t_w, mm	Y_7	0.0508
8[a]	TR	Y_8	$0.01Y_8$
9	H_1, mm	30.48	2.54
10	L, mm	5486.4	3.048
11	l, mm	3657.6	1097.3
12	p, N/mm	5.837	1.751
	2024-T3 extrusion		
13	Young's modulus, kN/mm^2	74.47	3.72
14	Allowable tensile strength, N/mm^2	351.65	17.93
15	Allowable compressive strength, N/mm^2	289.59	11.93
	2024-T3 bare sheet		
16	Young's modulus, kN/mm^2	72.40	3.62
17	Poisson's ratio	0.33	0.0165
18	Allowable tensile strength, N/mm^2	339.92	5.93

[a]Independent design variable.

The last column in Table 1 lists the standard deviation values for all random variables, with all except three held fixed during optimization. For w_3, t_3, and TR, standard deviation values represent the dependent design variables in the problem. The procedure for the calculation of standard deviation representing design uncertainty in each category is as follows.

Geometric Uncertainty

For a structural dimension specified as $Z^{+\Delta_u}_{-\Delta_l}$ with tolerance $(\Delta_u + \Delta_l)$ as the only available measure of variability, the standard deviation can be estimated using the relationship[19]

$$\tilde{\sigma}_X = (\Delta_u + \Delta_l)/F \tag{12}$$

where parameter F depends on sample size or the number of parts (NP) produced. For example, for NP of 25, $F = 4$, whereas $F = 5$ for NP of 100 (Ref. 19). While quantifying dimensional uncertainty, Eq. (12) also provides a link between manufacturing and structural reliability as the manufacturing process establishes the natural (i.e., achievable) tolerance for each part dimension.

For the spar caps, the specified tolerance and hence the standard deviation for each dimension are dictated by the end milling process.[20] Thus, for random variables 1–4 in Table 1, the standard deviation values are estimated using Eq. (12) based on a total of 100 spar caps (i.e., $F = 5$) and $\Delta_u = \Delta_l = 0.0635$ mm.

For extruded parts, such as the web stiffeners, that do not require any machining operation, the allowable tolerances for flange thickness and width (t_3, w_3) are specified as $\pm 2.5\%$ of the corresponding nominal values.[21] Thus, the standard-deviation values for random variables 5 and 6 are expressed as a function of respective mean values based on the specified tolerance and $F = 5$.

The initial size of the Tee extrusions and the final machined dimensions of the spar caps are correlated assuming the optimal dimensions at the root section are 90% of the original extrusion dimensions. In the case of the web stiffeners, because they do not require any machining, their optimal and extruded dimensions are assumed to be the same with the understanding that in order to use a standard size extrusion the actual dimensions can be slightly larger than the optimal values.

For web thickness t_w, the standard deviation is estimated using $F = 5$ and $\Delta_u = \Delta_l = 0.127$ mm, which is based on the precut size of the aluminum sheet and the expected range of thickness for each web segment.[18]

For the cap taper ratio, we assumed a coefficient of variation of 10%, and for spar height H_1 and length L, which are influenced by the assembly process, we chose tolerance limits of ± 6.35 and ± 7.62 mm resulting in standard deviation values of 2.54 and 3.048 mm, respectively.

Therefore, the standard deviation values for random variables 5, 6, and 8 represent dependent design variables as they are functions of the corresponding mean values (i.e., independent design variables).

Loading Uncertainty

Because the external load is usually subject to a greater scatter (i.e., uncertainty), we assumed a coefficient of variation of 30% for loading parameters l and p (see Fig. 1a).

Material Uncertainty

The mean values for Young's modulus and Poisson's ratio, in Table 1, are obtained from MIL-HDBK-5G with the coefficients of variation at 5% (Ref. 22). In the case of allowable tensile and compressive stresses, the A- and B-basis values for yield strength given in MIL-HDBK-5G are used to estimate the mean value and standard deviation for each allowable stress as[18]

$$\mu_{\sigma_Y} = 2.32\sigma_{Y_B} - 1.32\sigma_{Y_A} \tag{13}$$

$$\tilde{\sigma}_{\sigma_Y} = \frac{\sigma_{Y_B} - \sigma_{Y_A}}{1.158} \tag{14}$$

Web Design Concepts

Two different web design concepts are considered. In concept 1, the spar web is assumed to be in the state of pure shear and is limited in resistance by the shear buckling strength in each web panel, whereas in concept 2 it is allowed to go beyond buckling into the diagonal semitension field state. The difference in web design influences the loading conditions in the caps and the web stiffeners resulting in distinctly different failure modes that can greatly impact the optimal design for each concept. In both design concepts, the longitudinal spacing of web stiffeners, which can vary from one segment to another, is specified prior to performing the sizing optimization. The spacing variation can enhance design efficiency and lower manufacturing cost by reducing part count. As part of the weight-reliability-cost trade study, the optimization problem is solved for different number and spacing of web stiffeners with details discussed later in the paper.

Concept 1: Nonbuckling Web Design

In this concept, the spar caps are assumed to carry the entire bending as well as a portion of the transverse shear load as the spar height is tapered from root to tip. The web panel between two adjacent stiffeners is limited by its elastic shear buckling strength found as[23]

$$\tau_{\text{cr}} = \left[k_s \pi^2 E \big/ (1 - \nu^2)\right](t_w/b_w)^2 \tag{15}$$

where k_s represents the shear buckling coefficient, E the Young's modulus, ν the elastic Poisson's ratio, t_w the web thickness, and b_w the short dimension of a rectangular panel based on the average dimensions of the tapered panel.

When the spar is installed inside the wing, its caps are braced by the spar web along their vertical flanges and by the wing skin along the other flanges. Therefore, from the standpoint of static strength the lower (tension) cap is limited by the allowable tensile strength σ_{Y_t} (in lieu of fracture strength) of the material, whereas the upper (compression) cap is limited by its local crippling strength σ_{cs_c}, which is estimated using the semi-empirical equation for Tee sections given by Gerard[23] as

$$\sigma_{\text{cs}_c} = 0.67\sigma_{Y_c}\left[\left(3t^2_{\text{av}} \big/ A_c\right)(E/\sigma_{Y_c})^{0.5}\right]^{0.4} \tag{16}$$

where A_c is the cross-sectional area and t_{av} the weighted average wall thickness of the spar caps. For a Tee section, the crippling strength is generally limited to 80% of σ_{Y_c}, the compressive yield strength of the

material. In calculating its compressive failure strength, the upper spar cap is assumed to be under axial loading with no eccentricity.

The minimum allowable moment of inertia for web stiffeners placed only on one side of the shear-resistant web is found as[23]

$$I_{\mathrm{st_{all}}} = \frac{2.29 d_{\mathrm{st}}}{t_w}\left(\frac{V h_w}{33E}\right)^{\frac{4}{3}} \tag{17}$$

where d_{st} is the stiffener spacing, h_w is the average height of the web panel, and V is the transverse shear force at stiffener location. To keep the web stiffeners identical in size, the required moment of inertia is based on the most critical stiffener, which in this case is that located near the root.

Two rows of fasteners are used for cap-web and cap-stiffener assembly with longitudinal spacing determined based on the average shear flow in the two vertically adjacent fasteners as well as the fastener size, type, and the allowable shear strength. Because of spanwise variation in transverse shear force, the fastener spacing can vary from one panel to another, but it is kept fixed over each panel and is limited to a maximum of 50.8 mm. The web stiffeners are attached to the web by a single row of fasteners with vertical spacing calculated based on the average shear stress in the web at each stiffener location, and it is also limited to a maximum of 50.8 mm.

As was mentioned earlier, only the thickness of web segment 1 (see Fig. 1a) is treated as an independent design variable, with the thickness in each of the other two web segments calculated by setting the ratio of shear buckling strength to the average applied shear stress in the first panel of segments 2 and 3 (i.e., panels B and C) equal to that in panel A (see Fig. 1c). While reducing the number of independent design variables, this approach is shown to preserve the required structural reliability for all three web segments.

Hence, four critical elements in concept 1, as identified in Fig. 1c, are used for component reliability calculations with the limit state function for each component defined by the general formula

$$g_i(\boldsymbol{X}) = 1 - \eta_{i_{\mathrm{app}}}/\eta_{i_{\mathrm{all}}}, \qquad i = 1 \quad \text{to} \quad 4 \tag{18}$$

where $\eta_{i_{\mathrm{app}}}$ and $\eta_{i_{\mathrm{all}}}$ are functions of at least a subset of random variable vector $\boldsymbol{X}$, and for $i = 1$, they, respectively, refer to the applied shear stress τ and shear buckling strength τ_{cr} in panel A (see Fig. 1c); for $i = 2$, the applied stress σ_{lc} and tensile yield strength σ_{Y_t} in segment L1 of the lower cap; and for $i = 3$, the applied stress σ_{uc} and crippling strength σ_{cs_c} in segment U1 of the upper cap. In the case of web stiffeners, Eq. (18) is also used but after inverting the quotient such that $\eta_{4_{\mathrm{all}}}$ and $\eta_{4_{\mathrm{app}}}$ represent the minimum allowable $I_{\mathrm{st_{all}}}$ and actual moments of inertia in stiffener S2 (see Fig. 1c), respectively.

Concept 2: Buckling Web Design

In this concept, spar web panels are allowed to go beyond elastic buckling into diagonal semitension field state. The applied shear stress τ is expressed as the sum of τ_S caused by true shear and τ_{DT} caused by diagonal-tension action, where $\tau_S = (1-k)\tau$ and $\tau_{\mathrm{DT}} = k\tau$, with k known as the diagonal-tension factor. When $\tau > \tau_{\mathrm{cr}}$, k is found using the formula[24]

$$k = \tanh[0.5 \log_{10}(\tau/\tau_{\mathrm{cr}})] \tag{19}$$

For $\tau \le \tau_{\mathrm{cr}}$, the web is in the state of true shear, and $k = 0$.

The maximum applied shear stress in a web panel is calculated as[24]

$$\tau_{\max} = \tau\left(1 + k^2 C_1\right)(1 + kC_2) \tag{20}$$

where C_1 is a correction factor, which allows the diagonal tension field angle α to be less than 45 deg, and C_2 accounts for stress concentration as a result of flexibility of the spar caps. Because of taper in the spar web, τ is calculated based on the portion of transverse shear force carried by the web. The values of C_1 and C_2 are approximated using analytical models based on the corresponding graphs in Ref. 24.

Because the web is mechanically fastened to the caps and stiffeners, its allowable shear stress is calculated using Wagner's modified method[23] as

$$\tau_{\mathrm{all}} = \tau_{\mathrm{cr}} + (\sigma_{Y_t} - \tau_{\mathrm{cr}}/K_r) K_r R \sin\alpha \cos\alpha \tag{21}$$

The second term on the right-hand side of Eq. (21) represents the contribution of diagonal tension to shear strength, where K_r is the fastener correction factor and R is a factor similar to C_2 in Eq. (20) that depends on the web stiffener spacing, moments of inertia of the spar caps, and α (Ref. 23). Therefore, for the web panels the limit state function is expressed as

$$g_w = 1 - \tau_{\max}/\tau_{\mathrm{all}} \tag{22}$$

The primary normal stresses in the upper (compression) and lower (tension) caps are found as[23]

$$\sigma_{p_{\mathrm{uc}}}, \sigma_{p_{\mathrm{lc}}} = (1/A_{\mathrm{cap}})[\mp(M/\bar{h}) - (V_t/2)\cot\alpha] \tag{23}$$

where the first term on the right-hand side represents the stress caused by flexure, and the second is that caused by diagonal tension, with M representing the bending moment, $\bar{h}$ the vertical distance between centroids of the upper and lower caps, and V_t the portion of transverse shear force carried in tension field action.

The secondary normal stresses in the caps are created as a result of diagonal tension pulling the caps toward each other. In this case, the caps behave as continuous beams with the web stiffeners acting as support points. The secondary normal stresses in the upper and lower caps are found as[23]

$$\sigma_{s_{\mathrm{uc}}}, \sigma_{s_{\mathrm{lc}}} = \frac{y_c}{I_c}\left[\frac{C V_t d^2}{12h}\tan\alpha\right] \tag{24}$$

The bracketed term represents the secondary bending moment acting on the caps with the coefficient C defined as Wagner's relieving factor, d as stiffener spacing, and h as the vertical distance between centroids of the upper and lower cap-web fasteners. I_c denotes the moment of inertia of each cap, and y_c the vertical distance measured from the cap's centroid. The secondary bending moment is such that the bottom fiber of the upper cap and the top fiber of the lower cap are placed in compression.

For the upper cap, the bottom fiber is under the greatest compressive stress, whereas for the lower cap the bottom fiber sees the greatest tensile stress. Hence, the limit state function for the spar caps is expressed as

$$g_c = 1 - \sigma_{\max}/\sigma_{\mathrm{all}} \tag{25}$$

where $\sigma_{\max}$ represents the sum of primary and secondary normal stresses in each cap, with the lower cap limited by the tensile yield strength of the material and the upper cap limited by its crippling strength.

As for the web stiffeners, the tension field action puts them under axial compression with an average normal stress calculated as[23]

$$\sigma_{\mathrm{st}} = \frac{k\tau\tan\alpha}{A_{\mathrm{st}_e}/d_{\mathrm{st}}t_w + 0.5(1-k)} \tag{26}$$

where A_{st_e} is the effective stiffener area. The limit state function for the web stiffeners is similar to Eq. (25) with the allowable stress calculated using the Johnson–Euler equation[23]

$$\sigma_{\mathrm{st_{all}}} = \sigma_{\mathrm{cs_{st}}}\left[1 - \frac{\sigma_{\mathrm{cs_{st}}}}{4\pi^2 E}\left(\frac{L_{\mathrm{st}}}{\rho_{\mathrm{st}}}\right)^2\right] \tag{27}$$

where $\sigma_{\mathrm{cs_{st}}}$ is the crippling strength of the stiffener, L_{st} its length, and ρ_{st} its radius of gyration about the centroidal axis parallel to the web. For small values of slenderness ratio $L_{\mathrm{st}}/\rho_{\mathrm{st}}$, the allowable compressive strength is equal to the crippling strength of the stiffener.

Besides the main structural components, fastener design is also influenced by the semitension field design. Although in concept 2

the cap-web fasteners are subject to a shear load that is $(1+0.414k)$ times greater than that in concept 1, the stiffener-web fasteners are subject to a combination of shear and tensile stresses.[23] In this case, the fastener spacing is also limited to a maximum of 50.8 mm.

The failure modes in the four critical members shown in Fig. 1c are also used for component reliability analysis in concept 2.

Optimization Problem Formulation

The wing-spar design optimization problem is to find the optimal values of design variables that would

$$\begin{aligned}
&\min \quad \mu_W(\boldsymbol{Y}) \\
&\text{s. t.} \qquad g^c = 1 - \frac{\text{TMC}}{\text{TMC}_{\text{all}}} \geq 0 \\
&g_i^f = \frac{\beta_i^f}{\beta_{\min}} - 1 \geq 0, \qquad i = 1 \quad \text{to} \quad 4 \\
&g_j^m = 1 - \frac{\text{MF}_{\text{j}}}{\text{MF}_{\text{j}_{\text{all}}}} \geq 0, \qquad j = 1 \quad \text{to} \quad 6 \\
&g_k^a = \frac{\text{AF}_k}{\text{AF}_{k_{\text{all}}}} - 1 \geq 0, \qquad k = 1 \quad \text{to} \quad 3 \\
&g^d = 1 - \frac{\delta}{\delta_{\text{tip}}} \geq 0 \\
&Y_l^l \leq Y_l \leq Y_l^u, \qquad l = 1 \quad \text{to} \quad 8
\end{aligned} \tag{28}$$

where the objective function being minimized is the mean or expected value of spar weight. There are 15 design constraints and eight independent design variables. The constraint g^c imposes an upper-bound limit on the total manufacturing cost TMC, which is calculated according to the procedure described earlier and based on data obtained from MC/DG reports.[7–10] In calculation of TMC, the spar parts are assumed to involve no special or additional shop operation; hence, $\text{DICE}_p = 0$. Also, the cost associated with TI&E is usually very small and is ignored in this example. What remains are essentially the recurring and nonrecurring manufacturing costs of all discrete parts (i.e., machining cost of the caps and cutting costs of the web panels and web stiffeners) plus the cost of spar assembly, which is dominated by the number of fasteners used. Without focusing on any single cost element, a constraint is placed on TMC obtained using Eq. (7). The effect of this constraint on optimal design is examined and discussed later in the Results section.

The next four constraints impose lower-bound limits on the reliability index β associated with failure probability in the critical members: cap elements U1 and L1, panel A, and web stiffener S2 (see Fig. 1c) with corresponding limit state functions defined by Eq. (18) for concept 1, and by Eqs. (22) and (25) for concept 2. Taking panel A in concept 1 as an example, the reliability index is related to failure (i.e., buckling) probability through the relationship $\beta_{\text{web}} = \Phi^{-1}(1 - P_{f_{\text{web}}})$, where $P_{f_{\text{web}}} = P[(1 - \tau/\tau_{\text{cr}}) \leq 0]$. In this research, we used the Rackwitz–Fiessler[17] (R-F) implementation of AFOSM method for the calculation of each β with the minimum reliability or target reliability index chosen to be the same for all four critical members. The R-F method has been used extensively in the literature, and for linear to moderately nonlinear limit state functions in conjunction with random variables that have relatively low coefficients of variation and normal or lognormal distributions, as is the case here, it is shown to give fairly accurate estimates of β. Nonetheless, because of the linear approximation of the limit-state functions in the failure constraints and finite difference estimation of corresponding partial derivatives, there might be a small (typically $\sim$10% or less) error in the calculated values of β. At low values of β, the error that is propagated to the estimated failure probability P_f is not that significant because P_f tends to be rather high; however, at high values of β, even a small error in β can result in a significant underestimation of P_f.

There are six constraints limiting the values of six different manufacturing factors MF. The first three factors are the section balance SB, shape factor SF, and form factor FF for the Tee extrusions, whereas the next three are the same factors for the angle extrusions. The corresponding maximum allowable limits are $\text{SB}_{\text{all}} = 0.05$, $\text{SF}_{\text{all}} = 21$ obtained from Ref. 25, and $\text{FF}_{\text{all}} = 60$ obtained from Ref. 21. In addition, there are three constraints that impose lower bounds on assembly factors AF that consist of limits on the widths of cap's vertical and horizontal flanges as well as web stiffener flanges. For example, the vertical flange of each cap has to be wide enough to accommodate two rows of fasteners with a diameter of 6.35 mm. Furthermore, according to the limits specified by Niu,[26] the lower bound on dimension w_2 (see Fig. 1b) is set at $7D + \text{CR}$, where D is the fastener diameter and CR is the corner radius, which is assumed to be equal to the weighted average of t_1 and t_2 (see Fig. 1b).

The last design constraint imposes an upper-bound limit of 203.2 mm (i.e., approximately 4% of spar length) on the vertical tip displacement. In this example problem, the tip displacement is calculated using the unit-load method by considering only the contribution of bending moment to the strain energy with the resulting integral equation solved using the trapezoidal rule. In the calculation of flexural rigidity, the spar caps are assumed to provide the entire bending rigidity.

Because the nonlinear optimization problem in Eq. (28) is solved iteratively and the calculation of a reliability index in each iteration cycle requires the solution of the optimization problem in Eq. (3), only the g^f constraints with influence on structural safety are treated as probabilistic in order to save on computational time. The other constraints are modeled as deterministic by imposing limits on the mean values of the respective response variables. However, it would not be difficult to add any of the deterministic constraints to the list of reliability constraints. For example in the case of manufacturing cost, the probability of cost overrun would be expressed as $P_{f_{\text{cost}}} = P[(1 - \text{TMC}/\text{TMC}_{\text{all}}) \leq 0]$ with the corresponding reliability index estimated the same way as for the others. For any response variable of interest denoted by λ, we can estimate the standard deviation by using the chain-rule formula given as

$$\tilde{\sigma}_\lambda = \sqrt{\sum_{i=1}^{n} \left(\frac{\partial \lambda}{\partial X_i} \right)^2 \tilde{\sigma}_{X_i}^2} \tag{29}$$

where λ could represent weight, manufacturing cost, tip deflection, etc., and $\partial\lambda/\partial X_i$ its corresponding partial derivative with respect to the ith random variable.

Results and Discussion

After an extensive modification, the deterministic code TASPI[12] was used to obtain the optimization results presented here. The revised code, TASPI-Pro, solves the probabilistic design optimization problem in Eq. (28) by linking the design analyses discussed earlier with the general-purpose optimization code, DOT.[27] The results presented next are obtained using the method of sequential quadratic programming and do not necessarily represent the global optimal design for each design case. The solutions are presented for $\beta_{\min} = 1.29$ and 3.72, representing an approximate component failure probability of 1 in 10 and 1 in 10,000, respectively.

In concept 1, a minimum of seven web stiffeners, with distribution shown in Fig. 1c, was necessary to obtain a feasible design. With two evenly spaced intermediate stiffeners, segment 1 has three panels, whereas segment 2 has two panels with one intermediate stiffener, and segment 3 has just a single panel. Later, we also discuss the results when the number of intermediate stiffeners in each web segment is increased.

The optimization results for concept 1 at two different values of target reliability index $\beta_{\min}$ are shown in Table 1. Also to investigate the influence of cost constraint, the optimization problem is solved first without any limit on cost, and then it is solved again by requiring TMC to be no greater than 90% of its value found in the previous optimization problem. The standard deviation values for spar weight and cost are obtained from Eq. (29).

Table 2 Summary of optimization results for concepts 1 and 2

	Concept 1				Concept 2			
	Weight, kg		Cost, l-hr		Weight, kg		Cost, l-hr	
$\beta_{\min}$	μ_W	$\tilde{\sigma}_W$	μ_{TMC}	$\tilde{\sigma}_{\text{TMC}}$	μ_W	$\tilde{\sigma}_W$	μ_{TMC}	$\tilde{\sigma}_{\text{TMC}}$
Without cost constraint								
1.29	31.7	0.37	66.9	0.08	28.3	0.25	67.0	0.09
3.72	65.5	0.42	88.0	0.17	49.8	0.30	80.3	0.14
With cost constraint								
1.29	38.7	0.40	60.2	0.13	32.9	0.28	60.3	0.13
3.72	71.2	0.46	79.2	0.23	54.9	0.31	72.4	0.20

Table 3 Mean weight and cost distributions for concepts 1 and 2 at $\beta_{\min} = 3.72$

	Concept 1		Concept 2	
Component	Weight, kg	Cost, l-hr	Weight, kg	Cost, l-hr
Without cost constraint				
Caps	56.5	40.30	44.6	32.60
Webs	7.7	0.79	4.9	0.79
Stiffeners	1.3	1.12	0.3	1.12
Assembly	——	45.83	——	45.83
With cost constraint				
Caps	62.4	31.46	50.0	24.66
Webs	7.7	0.79	4.6	0.79
Stiffeners	1.1	1.12	0.3	1.12
Assembly	——	45.83	——	45.83

The most notable aspect of the results in Table 2 is the influence of $\beta_{\min}$. The tightening of target reliability index from 1.29 to 3.72 reduced the maximum failure probability in each component from 0.1 to 0.0001, but caused the spar weight to increase by 84 and 106% with and without the cost constraint, respectively. Also the optimal design at 90% of the cost leads to a weight increase of 22% for $\beta_{\min} = 1.29$ and 8.8% for 3.72.

The weight and cost breakdowns for concept 1 at $\beta_{\min} = 3.72$ are shown in Table 3. These results are based on a total of 12 parts (i.e., two caps, three web segments, and seven stiffeners) and 465 fasteners. It is evident that although the spar caps are the most significant contributor to the spar weight, they together with assembly are the primary contributors to TMC. The influence of cost constraint is that it reduces the taper ratio in the horizontal flanges of the caps, thereby reducing their machining cost, which is calculated based on the amount of material removed from the original extrusion as indicated by Eqs. (8) and (9). The reduction in taper ratio also causes the caps to become heavier, which in turn increases the spar weight.

When $\beta_{\min} = 1.29$, the manufacturing cost of the caps is 19.08 l-hr for approximately 29% of TMC (66.9 l-hr), whereas when $\beta_{\min}$ is increased to 3.72 that cost fraction increases to nearly 46% of TMC. However, the change in $\beta_{\min}$ has no impact on manufacturing cost of the web and the supporting stiffeners as well as the cost of spar assembly as the number of fasteners remains the same. The ratios of recurring to nonrecurring cost for the caps, web, stiffeners, and assembly are found to be 10.2, 5.6, 13, and 12.5, respectively, indicating that the recurring cost constitutes a much larger portion of total manufacturing cost.

Table 4 identifies the active set of design constraints at the optimal design point for concept 1. In addition to cost, the list also includes three of four reliability and three of nine manufacturability constraints. The physical-bound constraints address the assembly requirements by allowing adequate space for fastener placement. The tip displacement constraint is not active because of the large size of spar caps necessary to satisfy the reliability constraint in the upper cap. Table 5 lists the optimal values of design variables for concept 1 at both values of $\beta_{\min}$ with and without the cost constraint. As indicated earlier, Y_8, representing the mean value of the TR, appears to be the one most influenced by the cost constraint.

The results for concept 2 are also shown in Table 2, and, similar to concept 1, a minimum of seven intermediate stiffeners was needed to achieve a feasible design (see Fig. 1c). This design was also optimized with and without the cost constraint for both values of $\beta_{\min}$.

Table 4 Active and inactive design constraints for concepts 1 and 2

		Concept	
Constraint type	Constraint definition	1	2
g^c	Total manufacturing cost	A	A
g_1^f	Upper-cap reliability index	A	A
g_2^f	Lower-cap reliability index	I	A[a]
g_3^f	Web reliability index	A	A
g_4^f	Stiffener reliability index	A	I
g_1^m	Cap SB	A	A
g_2^m	Cap SF	I	I
g_3^m	Cap FF	I	I
g_4^m	Stiffener SB	I	I
g_5^m	Stiffener SF	A	A
g_6^m	Stiffener FF	I	I
g_1^a	Manufacturing bound on w_2	A	A
g_2^a	Manufacturing bound on w_1	I	I
g_3^a	Manufacturing bound on w_3	I	A
g^d	Maximum tip displacement	I	I

[a]Only at $\beta_{\min} = 3.72$.

Table 5 Optimal values of design variables in concepts 1 and 2

Design variable	Random variable	Concept 1		Concept 2	
		$\beta_{\min} = 1.29$	$\beta_{\min} = 3.72$	$\beta_{\min} = 1.29$	$\beta_{\min} = 3.72$
		Without cost constraint			
Y_1	w_1, mm	152.40[a]	152.40[a]	106.70	152.40[a]
Y_2	t_1, mm	8.13	16.00	8.64	13.46
Y_3	w_2, mm	51.56	58.67	52.07	56.13
Y_4	t_2, mm	3.53	9.60	5.84	7.37
Y_5	w_3, mm	49.53	49.53	15.24	15.49
Y_6	t_3, mm	2.51	3.07	2.64	2.67
Y_7	t_{web}, mm	2.31	2.67	1.32	1.65
Y_8	TR	0.30[b]	0.30[b]	0.30[b]	0.30[b]
		With cost constraint			
Y_1	w_1, mm	147.30	152.40[a]	106.68	106.68
Y_2	t_1, mm	8.00	15.75	8.38	13.97
Y_3	w_2, mm	51.31	58.42	52.07	57.40
Y_4	t_2, mm	3.73	9.42	5.84	10.92
Y_5	w_3, mm	49.78	52.83	15.24	15.24
Y_6	t_3, mm	2.49	2.49	2.64	2.64
Y_7	t_{web}, mm	2.31	2.67	1.35	1.57
Y_8	TR	0.62	0.46	0.59	0.48

[a]Upper bound. [b]Lower bound.

As expected, the use of buckling-type web design in concept 2 allows the spar weight to decrease by an average of 14.3% over the range of $\beta_{\min}$ considered. Although there is no significant difference between the costs of the two concepts at $\beta_{\min} = 1.29$, concept 2 becomes less expensive with an increase in $\beta_{\min}$ such that at $\beta_{\min} = 3.72$ it is 8.6% cheaper to build than concept 1 if the number of parts and fasteners are kept the same. This cost reduction is made possible only through reduced machining cost of the spar caps. The examination of optimal weight and the corresponding cost vs $\beta_{\min}$ for the case without the cost constraint reveal that weight escalates at a much faster rate than cost as $\beta_{\min}$ is increased.

The weight and cost distributions for concept 2 are also shown in Table 3 with the number of parts and fastener count the same as in concept 1. The active constraint set at the optimal design point is also given in Table 4. In addition to cost, the list also includes three out of four reliability constraints and four out of nine manufacturability constraints.

Table 5 shows the optimal values of design variables for concept 2 at both values of $\beta_{\min}$ with and without the cost constraint. The design variable most influenced by the cost constraint is once again Y_8, the mean taper ratio. However, by increasing the $\beta_{\min}$ value, Y_1

Table 6 Effect of NS on optimal spar design

NS in segment			Concept 1		Concept 2	
1	2	3	Weight, kg	Cost, l-hr	Weight, kg	Cost, l-hr
2	1	0	65.5	88.0	49.8	80.3
3	2	1	65.7	90.9	48.1	83.2
4	3	2	66.0	93.9	48.2	86.1
5	4	3	66.4	96.9	48.3	89.1
6	5	4	66.5	99.9	48.5	92.2

Table 7 Effect of NS in concept 2

NS in segment					
1	2	3	k	Y_7, mm	τ/τ_{cr}
2	1	0	0.080	1.65	1.44
3	2	1	0.357	1.07	5.58
4	3	2	0.358	1.01	5.62
5	4	3	0.353	1.00	5.47
6	5	4	0.332	1.00	4.91

and Y_4 are also influenced by the inclusion of cost constraint. The most obvious difference between concepts 1 and 2 appears to be in the mean web thickness Y_7, mean stiffener-width Y_5, and the mean vertical flange thickness of the caps Y_4.

The tightening of target reliability index from 1.29 to 3.72 caused the weight to increase by an average of 90% for concept 1 and 70% for concept 2 and increased TMC by more than 30 and 20%, respectively, both primarily as a result of growth in spar cap dimensions. The assembly cost stayed constant, however, because of no change in the number of fasteners. A closer examination revealed that the use of 50.8 mm as maximum fastener spacing was the reason. If this limit were removed, then the number of fasteners for concept 1 would have been less than that for concept 2.

The effect of stiffener spacing was also investigated with the results shown in Table 6. Theoretically, the shear-buckling coefficient increases asymptotically as the panel aspect ratio approaches one. Therefore, by adjusting stiffener spacing it is possible to increase the buckling coefficient and allow the panel to become thinner while maintaining the desired buckling strength. The results in Table 6 are for different values of NS representing the number of evenly spaced intermediate stiffeners in web segments 1–3. For all of the cases in Table 6, β_{min} is kept at 3.72, and the design is optimized without the cost constraint. As expected, for both concepts 1 and 2 the web thickness decreases as NS is increased. However, in concept 1 the increase in NS leads to a growth in the total spar weight because the weight gained through the addition of stiffeners is slightly greater than the weight saved by reducing the web thickness. By contrast, in concept 2 increasing NS leads to a rapid reduction in total weight followed by a gradual increase beyond what appears to be the optimal stiffener topology (among the combinations examined) at NS equal to 3, 2, 1 for segments 1, 2, and 3, respectively. Whereas in concept 1 the minimum weight design corresponds to the minimum cost design, in concept 2 it does not. The weight reduction of 1.72 kg (3.5%) in going from NS = 2, 1, 0 to NS = 3, 2, 1 in concept 2 is accompanied by a cost increase of 2.9 l-hr (3.6%).

The effect of NS in concept 2 is explored further with the help of Table 7. The shear-stress ratio in the last column gives an indication of the load carried by panel A near the fixed end. Although the largest k occurs in the case NS = 4, 3, 2, the lightest design corresponds to NS = 3, 2, 1. A closer examination of the results indicated that the size of web stiffeners has reached the constrained imposed by the manufacturability requirement and cannot become any smaller as their quantity increases. There is also a very minor change in the cap dimensions as a result of changing NS. So the fact that NS = 3, 2, 1 gives the lightest weight is caused by the combination of cap size and web thickness.

The optimization solutions had a slightly faster rate of convergence in concept 1 than concept 2. However, in all cases convergence was reached in less than 10 optimization cycles for an average CPU time of less than a minute on a Sun Ultra-4 Sparc workstation.

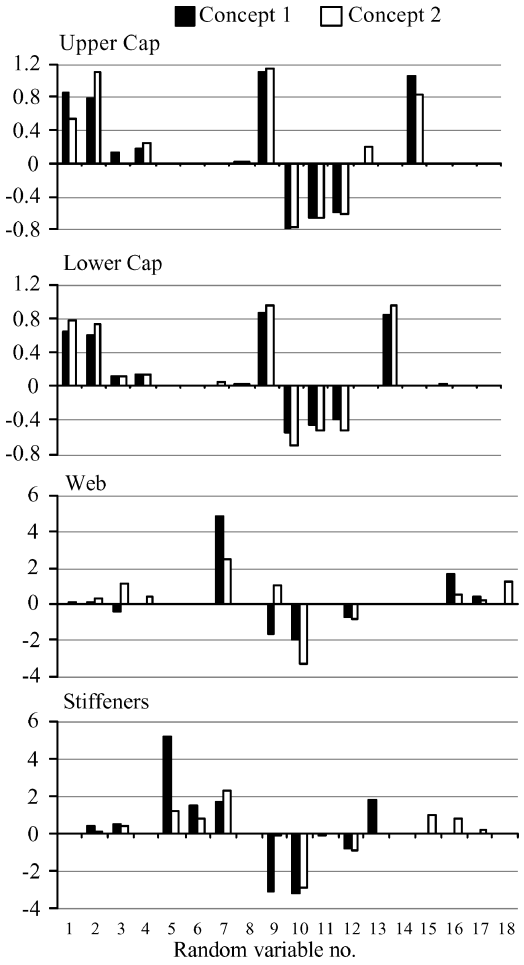

Fig. 2 Plot of reliability sensitivity derivatives obtained from Eq. (30a).

Design Sensitivity Analysis

Equations (4a) and (4b) are used to calculate the probabilistic sensitivity derivatives of each reliability index with respect to the mean value and standard deviation of individual random variables identified in Table 1. These sensitivities are calculated at the optimal design point and normalized as

$$\left.\frac{\partial\beta}{\partial\mu_{X_i}}\right|_{x^*}^{n} = \left.\frac{\partial\beta}{\partial\mu_{X_i}}\right|_{x^*}\left(\frac{\mu_{X_i}}{\beta}\right) \tag{30a}$$

$$\left.\frac{\partial\beta}{\partial\tilde{\sigma}_{X_i}}\right|_{x^*}^{n} = \left.\frac{\partial\beta}{\partial\tilde{\sigma}_{X_i}}\right|_{x^*}\left(\frac{\tilde{\sigma}_{X_i}}{\beta}\right) \tag{30b}$$

The plots of Eq. (30a) for concepts 1 and 2 are shown in Fig. 2. In the case of concept 1, the reliability of the upper cap is influenced most by the spar height at the root H_1 followed closely by the compressive yield strength of the cap material. For the lower cap H_1 and the tensile yield strength of the material have the most influence on β. For the web, the most influential random variable is the web thickness followed by the spar length, whereas for the web stiffeners the stiffener flange width has the most influence on stiffener reliability followed by spar length and height.

In the case of concept 2, the reliability of the upper cap appears to be most sensitive to the values of horizontal flange thickness and the spar height at the root followed by the compressive yield strength of the material. The effects of spar length and load parameters are also evident in these plots. The lower cap is slightly more sensitive to the spar height at the root and the tensile yield strength of the material than the horizontal flange dimensions. The influences of spar length and the load parameters are strong in this case as well but less so than for the upper cap. The influence of length is most pronounced on reliability of the web and web stiffeners followed by that of web thickness.

Table 8 Effect of RV distribution type on optimal values of design variables in concept 1 at $\beta_{min} = 3.72$

Design variable	Random variable	Normal	Log-normal
Y_1	w_1, mm	152.40[a]	152.40[a]
Y_2	t_1, mm	16.00	22.10
Y_3	w_2, mm	58.67	64.52
Y_4	t_2, mm	9.60	15.24
Y_5	w_3, mm	49.53	49.53
Y_6	t_3, mm	3.07	3.28
Y_7	t_{web}, mm	2.67	2.90
Y_8	TR	0.30[b]	0.30[b]

[a]Upper bound. [b]Lower bound.

Effect of RV Distribution Type

With the influence of random variables 9–12 (see Table 1) more widespread than others, we optimized the design in concept 1 again after changing the distribution type of these four random variables from normal to log-normal. The optimal design variables for the two cases are compared in Table 8. Using the log-normal distribution, the optimal mean weight and cost at $\beta_{min} = 3.72$ were found to be 97.3 kg and 101.5 l-hr, respectively, as compared to 65.5 kg and 88 l-hr for the normal distribution (see Table 2). The mean weights of caps, webs, and stiffeners are 87.7, 8.3, and 1.3 kg, respectively, and the mean costs for the caps, web, stiffeners, and assembly are found to be 54.0, 0.79, 1.12, and 45.67 l-hr, respectively. As indicated in Table 8, with random variables 9–12 having a log-normal distribution, the caps will need to be approximately 45% larger than before in order to satisfy the reliability constraint on the upper cap.

Conclusions

A methodology for probabilistic design optimization of aircraft structures in presence of structural reliability, manufacturability, and manufacturing cost constraints was presented. Design uncertainties caused by variations in structural dimensions, material properties, and loading condition were considered in the application of this methodology to a wing-spar problem with two alternative web design concepts. The design constraints were evaluated using analytical and semi-empirical methods that also facilitated the modeling of relationships between design variables and parameters defining the capabilities of the manufacturing process and the production costs. The optimization results were used to explore tradeoffs between reliability, weight, and cost, whereas the probabilistic sensitivities were used to examine the influence of each random variable on the reliability of spar components.

Of all design constraints, cost and component reliability were found to be the most influential. The main influence of the cost constraint was to increase the cap taper ratio thereby reducing its machining cost. Among the manufacturability constraints, section balance had the most influence on the cap design. The use of buckling-type web design in concept 2 reduced the overall weight of the spar as the web was allowed to carry shear beyond buckling in the form of diagonal semitension field action. Although the weight in concept 2 was generally less than concept 1, there was no appreciable difference in the total manufacturing cost, which was dominated by the assembly process and the manufacturing cost of the spar caps. The tightening of target reliability index resulted in a greater weight than cost penalty in both design concepts. Furthermore, the reduction in stiffener spacing (i.e., increasing the number of intermediate stiffeners) resulted in a monotonic weight increase in concept 1, but for concept 2 the use of 10 stiffeners led to the lowest-weight spar design. Besides the mean value and standard deviation, the distribution type of spar height, spar length, and loading parameters also had a more significant impact on spar weight than cost.

Further investigation is needed to account for such important issues as fatigue and damage tolerance, which can prove to be equally or more important than the failure modes included here.

Acknowledgment

This work was supported in part by the Department of Aerospace Engineering at Mississippi State University.

References

[1]Gupta, S. K., Das, D., Regli, W. C., and Nau, D. S., "Current Trends and Future Challenges in Automated Manufacturability Analysis," Inst. for Systems Research, Univ. of Maryland, TR 95-16, College Park, MD, 1995.

[2]Kessler, W. C., Shumaker, G. C., and Hitchcock, M. F., "Early Manufacturing Considerations in Design," AGARD, Paper N94-24315, April 1993.

[3]Shankar, S. R., and Jansson, D. G., "A Generalized Methodology for Evaluating Manufacturability," *Concurrent Engineering, Contemporary Issues and Modern Design Tools*, Chapman and Hall, New York, 1993, pp. 248–263.

[4]Subramaniam, B. L., and Ulrich, K. T., "Producibility Analysis Using Metrics Based on Physical Models," *Design Theory Methodology*, DE-Vol. 68, American Society of Mechanical Engineers, 1994, pp. 353–369.

[5]Fenyes, P., "Structural Optimization with Manufacturing Considerations," *Proceedings of the 33rd AIAA/ASME/ASCE/AHS/ASC Structures, Structural Dynamics and Materials Conference*, Pt. 2, AIAA, Reston, VA, 1992, pp. 638–647.

[6]Dean, E. B., "Parametric Cost Analysis: A Design Function," *Transaction of the American Association of Cost Engineers 33rd Annual Meeting*, American Association of Cost Engineers, 1989.

[7]Noton, B. R., "ICAM: Manufacturing Cost/Design Guide," Final Rept., Vols. 1–3, U.S. Air Force Materials Lab., AFML-TR-76-227, Wright–Patterson AFB, OH, March 1979.

[8]Noton, B. R., "ICAM Manufacturing Cost/Design Guide," *Final Technical Report—Airframe User's Manual*, Vols. 1–3, U.S. Air Force Wright Aeronautical Labs., AFWAL-TR-83-4033, Wright–Patterson AFB, OH, Jan. 1983.

[9]Noton, B. R., "ICAM Manufacturing Cost/Design Guide, Vol. V—Machining," U.S. Air Force Wright Aeronautical Labs., AFWAL-TR-83-4033, Wright–Patterson AFB, OH, March 1985.

[10]Noton, B. R., "ICAM Manufacturing Cost/Design Guide, Volume I: Demonstration Sections," U.S. Air Force Wright Aeronautical Labs., AFWAL-TR-80-4115, Wright–Patterson AFB, OH, Sept. 1980.

[11]Frangopol, D., "Reliability-Based Optimum Structural Design," *Probabilistic Structural Mechanics Handbook, Theory and Industrial Applications*, Chapman and Hall, London, 1995, pp. 352–387.

[12]Rais-Rohani, M., and Huo, Z., "Analysis and Optimization of Primary Aircraft Structures Based on Strength, Manufacturability, and Cost Requirements," *Proceedings of the 40th AIAA/ASME/ASCE/AHS/ASC Structures, Structural Dynamics and Materials Conference* [CD-ROM], AIAA, Reston, VA, 1999.

[13]Martinez, M. P., Messac, A., and Rais-Rohani, M., "Manufacturability-Based Optimization of Aircraft Structures Using Physical Programming," *AIAA Journal*, Vol. 39, No. 3, 2001, pp. 517–542.

[14]Wu, Y.-T., "Computational Methods for Efficient Structural Reliability and Reliability Sensitivity Analysis," *AIAA Journal*, Vol. 32, No. 8, 1994, pp. 1717–1723.

[15]Shinozuka, M., "Basic Analysis of Structural Safety," *Journal of the Structural Division*, Vol. 109, No. 3, 1983, pp. 721–740.

[16]Hasofer, A. M., and Lind, N., "An Exact and Invariant First-Order Reliability Format," *Journal of Engineering Mechanics*, Vol. 100, No. 1, 1974, pp. 111–121.

[17]Rackwitz, R., and Fiessler, B., "Structural Reliability Under Combined Random Load Sequences," *Computers and Structures*, Vol. 9, No. 5, 1978, pp. 489–494.

[18]Madson, H. O., Krenk, S., and Lind, N. C., *Methods of Structural Safety*, Prentice–Hall, Englewood Cliffs, NJ, 1986, pp. 120–123.

[19]Haugen, E. B., *Probabilistic Mechanical Design*, Wiley, New York, 1980, pp. 91–188.

[20]Judson, T. W., "Parts Produced on Milling Machines," *Design for Manufacturability Handbook*, 2nd ed., McGraw–Hill, New York, 1998, pp. 4.59–4.71.

[21]Trucks, H. E., *Designing for Economical Production*, 2nd ed., Society of Manufacturing Engineers, Dearborn, MI, 1987, pp. 133–137.

[22]Dowling, N. E., *Mechanical Behavior of Materials*, 2nd ed., Prentice–Hall, Upper Saddle River, NJ, 1998, p. 803.

[23]Bruhn, E. F., *Analysis and Design of Flight Vehicle Structures*, S. R. Jacobs and Associates, Indianapolis, IN, 1972, Chaps. C5, C7, C10, and C11.

[24]Kuhn, P., Peterson, J. P., and Levin, L. R., "A Summary of Diagonal Tension: Part I—Methods of Analysis," NACA TN 2661, May 1952.

[25]Balasubramaniam, L., "Producibility Analysis Using Analytical and Empirical Process Models," Ph.D. Dissertation, Dept. of Mechanical Engineering, Massachusetts Inst. Technology, Cambridge, MA, Sept. 1993.

[26]Niu, M. C. Y., *Airframe Structural Design*, Conmilit Press, Ltd., Hong Kong, PRC, 1988, pp. 538–580.

[27]DOT, Design Optimization Tools, Ver. 5, Vanderplaats Research and Development, Colorado Springs, CO, Jan. 2001.

A. Messac
Associate Editor